Journal of Power Sources 189 (2009) 337–343

Contents lists available at ScienceDirect

Journal of Power Sources

journal homepage: www.elsevier.com/locate/jpowsour

Electrochemical properties and Li deposition morphologies of surface modified graphite after grinding

H. Honbo[a,*], K. Takei[b], Y. Ishii[c], T. Nishida[c]

[a] Materials Research Laboratory, Hitachi, Ltd., 7-1-1, Omika-cho, Hitachi-shi, Ibaraki, 319-1292 Japan
[b] Research & Development Center, Hitachi Chemical Co., Ltd., 3-3-1, Ayukawa-cho, Hitachi-shi, Ibaraki, 316-0036, Japan
[c] Development Division, Yamazaki Works (Sakuragawa), Hitachi Chemical Co., Ltd., 3-3-1, Ayukawa-cho, Hitachi-shi, Ibaraki, 316-0036, Japan

ARTICLE INFO

Article history:
Received 19 June 2008
Received in revised form 7 August 2008
Accepted 21 August 2008
Available online 27 August 2008

Keywords:
Lithium
Graphite
Dendrite
Irreversible capacity
R-value
Grinding

ABSTRACT

Electrochemical properties and Li deposition morphologies of several kinds of carbon with different surfaces were studied. The surface conditions and Li deposition morphologies were analyzed using Raman spectroscopy and scanning electron microscopy. It appeared that the disordered carbon surface suppressed the Li dendrite deposition. Grinding methods with different clearances were adopted to modify the graphite into a desirable surface. The *R*-value increased from 0.10 to 0.63 after grinding to 40 μm, though a significant change in d_{002} did not occur. These results suggest that disordered carbon was created on the surface without a significant change in bulk crystallinity. Thus, the reversible capacity, which is about 350 mAh g^{-1}, was the same before and after grinding. However, the Li deposition morphologies significantly changed before and after grinding. The pristine graphite had a dendritic morphology, but the ground graphite had a granular morphology. It is believed that the defects on the disordered carbon act as electrodeposition nuclei and prevent the formation of Li dendrites.

1. Introduction

Lithium-ion batteries (LIBs), with suitable lithium intercalation compounds for electrodes, have been used in various applications due to their higher voltage, higher energy density, and longer shelf life compared with conventional rechargeable batteries. LIBs usually consist of a lithium transition metal oxide for the cathode and a carbonaceous material for the anode. A continuous supply of these materials is needed to improve their properties, especially capacity, because the capacity demand of mobile devices, such as cellular phones and notebook computers, has increased rapidly. One issue of carbon anodes is the irreversible reaction during the first lithiation. Li consumed in the first cycle cannot be reversibly recovered and the excess cathode material to compensate for the consumed Li leads to a decrease in energy density. It is widely recognized that part of this irreversibility arises from electrolyte decomposition followed by the formation of a passivation layer or solid electrolyte interface (SEI) on the carbon surface [1,2]. Therefore, many researchers have made a number of efforts in searching for a good electrolyte that could reduce the irreversible reaction and analyzing the nature of SEI over the last decade [3,4]. Thus, it is believed that this irreversible reaction is affected by the structure of the carbon surface where electrolyte decompositions take place resulting in the development of several methods of carbon surface modification for reducing the irreversible reaction and to achieve a higher-energy density of LIBs [5,6].

On the other hand, the safety of LIBs has been the subject of focus because the energy density of LIBs increases greatly. In the past, the thermal decomposition reactions of lithiated carbon electrodes have been studied using differential scanning calorimetry (DCS) [7,8], accelerating rate calorimetry (ARC) [9,10], etc. It is generally known that decomposition reactions start around 120 °C, and they are affected by the stability of the SEI [11]. However, the mechanism of Li deposition on a carbon surface has hardy been studied, while dendritic Li, which is deposited on the carbon surface during overcharging, causes a serious decline in the safety of the LIB. It was reported that the melting of deposited Li and the resulting exothermic reactions may be significant contributors to cell rupture if the cell temperature rises over 180 °C [12].

It is believed that the surface structure of carbon has a great effect on not only SEI formations but also Li deposition morphologies. Therefore, we attempted to reduce the amount of dendritic Li by modifying the surface of graphite to improve the electrochemical property. While there are several kinds of surface modification methods, such as ballmilling [13–15], carbon coating [16], polymer

* Corresponding author. Tel.: +81 294 52 5111; fax: +81 294 52 7636.
E-mail address: hidetoshi.hombo.xu@hitachi.com (H. Honbo).

0378-7753/$ – see front matter © 2008 Elsevier B.V. All rights reserved.
doi:10.1016/j.jpowsour.2008.08.048

Table 1
Structural and electrochemical properties of carbon samples

Sample		d_{002} (nm)	Average diameter (μm)	BET surface area ($m^2\,g^{-1}$)	*R*-value (–)	Reversible capacity ($mAh\,g^{-1}$)	Irreversible capacity ($mAh\,g^{-1}$)
ID	Feature						
AG1	Artificial graphite	0.335	19	3.5	0.10	347	32
GM	Graphitized mesocarbon	0.336	24	0.6	0.46	300	13
AG2	Artificial graphite	0.337	11	1.7	1.0	326	21
AC	Amorphous carbon	0.37	12	4.4	1.4	299	50
AG1-100	AG1 ground in 100 μm	0.335	18	3.7	0.24	348	30
AG1-60	AG1 ground in 60 μm	0.335	20	3.7	0.30	348	26
AG1-40	AG1 ground in 40 μm	0.335	20	3.8	0.63	346	32

coating [17], and metal oxide treating [18], we chose the grinding method for surface modification because of its convenience.

2. Experiments

2.1. Carbon samples

Artificial graphite (AG1 and AG2), graphitized mesocarbon (GM), and amorphous carbon (AC) samples were used (Table 1). The average diameter range and Brunauer Emmett and Teller (BET) surface area range of these carbon samples were from 11 to 24 μm, and from 0.6 to 4.4 $m^2\,g^{-1}$, respectively. In these samples, AG1, which is a highly crystalline graphite structure and whose interlayer space (d_{002}) is 0.335 nm, was mechanically milled with a grinder (Masco, Supermasscolloider MKZA10-15) to create a disordered region on the graphite surface. The clearance between the two rotating Al_2O_3 grinders was from 40 to 100 μm.

The structural parameters of the carbon samples were analyzed with an X-ray diffractometer using Rigaku RU-200B with Cu Kα radiation. We evaluated the degree of surface crystallinity of the carbon samples with Raman spectroscopy using a RENISHAW Ramanscope (He–Ne laser, 633 nm, 25 mW) at room temperature. The ratio of peak intensity of about 1360 cm^{-1} to that of about 1580 cm^{-1}, the so called *R*-value, was used as a parameter reflecting the degree of surface crystallinity of the carbon samples. The surface disorder regions of these materials were removed by thermal analysis using SII DG/DTA6200 at a heating rate of 5 °C min^{-1} from room temperature to 900 °C. The surface morphologies of anodes made of these carbons were analyzed with scanning electron microscopy (SEM) using the Hitachi S-2460N.

2.2. Electrochemical tests

The carbon electrodes were made by mixing a slurry containing 5 wt% polyvinylidene fluoride (PVdF) binder (Kureha, KFL#1120) and 95 wt% carbon powder in a N-methyl-2- pyrrolidone (NMP) solution. The slurry was spread on a copper foil (18 μm thick) as a current collector using a doctor blade, and was dried in an oven at 80 °C to evaporate NMP. The coated foil was then roll-pressed into about 1.5 $g\,cm^{-3}$, and was cut into 1 cm^2. The typical weight of coated carbon materials is about 10 $mg\,cm^{-2}$. Before conducting the electrochemical test, the carbon electrodes were dried in a vacuum oven at 120 °C for 2 h.

The electrochemical tests were performed using three-electrode cells with working, reference, and counter electrodes in an argon dry box. In these cells, Li metal foils were used as both the reference and the counter electrodes, and carbon electrodes were used as the working electrodes. The electrolyte used was 1M $LiPF_6$ in ethylene carbonate (EC) and dimethyl carbonate (DMC) in a 1:2 volume ratio (Tomiyama Pure Chemical Industries). After soaking these electrodes and a separator film (Tonen Chemical, 25 μm thick) in the electrolyte, the working and counter electrodes were stacked with a separator film interposed between them, and the reference electrodes were placed on the side of the working electrode. These electrodes were then fastened at a constant pressure with two disk plates and bolts at 0.05 Nm with a torque wrench. This cell was enclosed in a glass vessel to avoid electrolyte evaporation.

Electrochemical Li intercalation and deintercalation tests were conducted using a cell tester (Toyo system, TOSCAT3100U) at 0.5 mA cm^{-2} between 0.005 and 2.0 V vs. Li/Li^+. Li electrodeposition was carried out galvanostatically at 8.5 mA cm^{-2} for 3 min after fully intercalating Li into a carbon electrode. The Li deposition morphologies were examined using SEM after rinsing the samples with DMC and dying adequately.

3. Results and discussion

3.1. Raman spectra and Li intercalation and deintercalation properties

Raman spectroscopy is a suitable method for examining surface conditions of carbon materials. Fig. 1 shows Raman spectra of the as received carbon samples. Two peaks around 1360 and 1580 cm^{-1} were observed in each spectrum of the carbon. It is generally known that a peak of 1580 cm^{-1} (G band) corresponds to in-plane vibrations of the carbon atoms in the hexagonal net plane of graphite and that of 1360 cm^{-1} (D band) originates from the disordered hexagonal structure of graphite [19].

The *R*-values of AG1, GM, AG2, and AC, which were 0.10, 0.46, 1.0 and 1.4, respectively, as shown in Table 1, indicates that the degree of disordered hexagonal structure increases in this order. At the same time, graphite interlayer space (d_{002}) of AG1, GM and AG2 were between 0.335 and 0.337 nm. This shows that the crystallinity of these graphite samples were extensively high. Raman spectroscopy is sensitive to surface conditions rather than the bulk

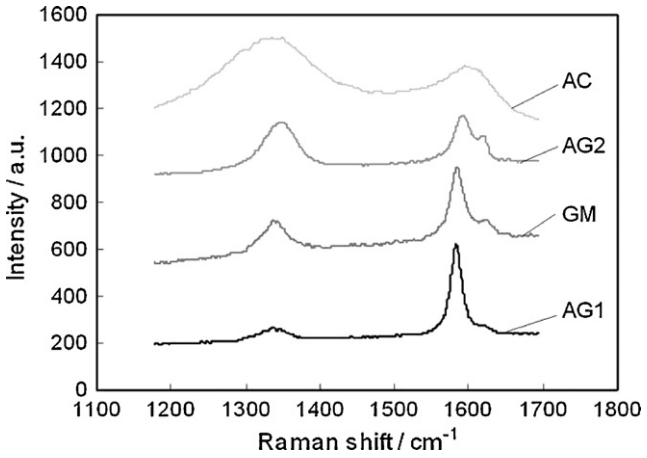

Fig. 1. Raman spectra profiles of carbon samples.

structure, so it was assumed that GM and AG2 had some disorder regions on their surface. This affected Li intercalation and deintercalation reversible capacities (C_{rev}), which AG1 was the maximum in these samples, as the amount of LiC_6 formed by Li intercalation into graphite increases depending on the degree of the crystallinity of graphite. The C_{rev} of AG1, GM, and AG2 were 347, 300, and 326 mAh g^{-1}, respectively. On the other hand, irreversible capacities (C_{irrev}) of these samples, as shown in Table 1, increased depending on the surface area of graphite due to occurring electrolyte decomposition on the surface [20] while C_{rev} and C_{irrev} of AC, which was an amorphous carbon sample, were 299 and 50 mAh g^{-1}, respectively. It is known that the irreversible reaction of amorphous carbon is different from that of graphite. The capacity of Li trapping inside amorphous carbon could also add to C_{irrev} [21].

3.2. Morphologies of Li deposition on carbon electrode

Li electrodepositions were carried out galvanostatically at 8.5 mA cm^{-2} (ca. 3 C rate) for 3 min after fully intercalating Li into AG1, GM, AG2 and AC, respectively. The capacity of Li electrodeposition was 45 mAh g^{-1}, and this value corresponded with 13 to 15% of the electrode reversible capacities. As shown Fig. 2, all of the electrode potentials went below 0 V immediately after overcharging, and this indicated that Li depositions occurred at all of the carbon electrodes. During Li deposition, the minimum potentials of AG1, GM, AG2 and AC were −0.44, −0.28, −0.20, and −0.20 V, respectively. This showed that the overcharge voltage of Li deposition decreased in order to increase the *R*-values.

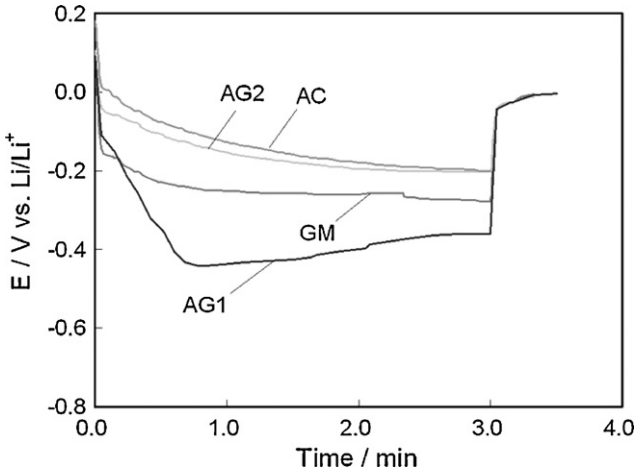

Fig. 2. Potential curves of AG1, GM, AG2, and AC during overcharge at 8.5 mA cm^{-2} for 3 min in 1 M $LiPF_6$ EC/DMC (1:2).

Fig. 3 shows SEM images of Li deposition morphologies on the above carbon electrodes. Dendritic Li deposition could be seen on AG1 (Fig. 3(a)) and GM (Fig. 3(b)) after overcharge. It seemed that

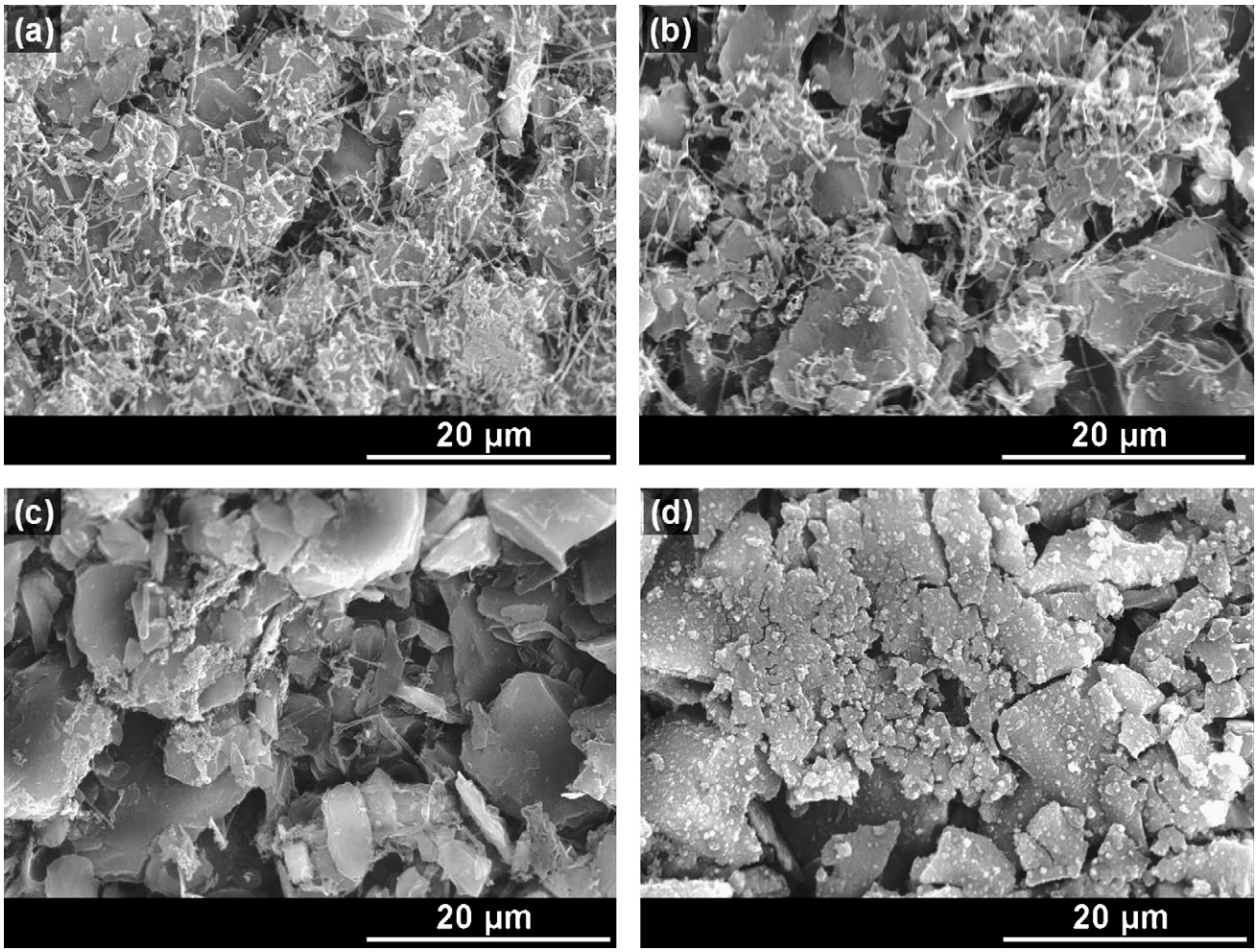

Fig. 3. SEM images of (a) AG1; (b) GM; (c) AG2; (d) AC after Li deposition.

the amount of dendritic Li deposition on AG1, of which surface was mostly crystalline, was more than that of GM, and there was some aggregated Li deposition on GM also. On the other hand, the amount of aggregated Li deposition increased and the dendritic Li deposition clearly diminished on AG2 (Fig. 3(c)), of which the *R*-value was more than 1.0. Furthermore, particle Li deposition could only be seen on AC (Fig. 3(d)), which was the amorphous carbon.

There were previous reports on Li deposition morphologies on Ni substrates containing 5×10^{-3} mol dm^{-3} HF in electrolyte, which markedly changed dendritic morphology into a smooth and uniform surface [22–24]. However, other factors were expected because the electrolyte we used in this work had very little HF content. It was assumed that the amount of nuclei, which are defects on a carbon surface, affect Li deposition morphologies because they are the origin points of Li depositions. Therefore, due to the increase in *R*-value, the amount of dendritic Li deposition on AG1, GM, AG2, and AC gradually decreased in this order.

At the same time, it was also assumed that Li intercalations into carbon under 5 mV vs. Li/Li$^+$, which was the cutoff potential before Li deposition, were involved in the overcharge capacity because the total amount of Li deposition was different for each sample, and those reactions would likely reduce the dendritic Li deposition and overcharge voltage. Although it is hard to say how much the amount of nuclei and the residual intercalation capacities in this study suppressed dendritic Li deposition and decreased overcharge voltage, respectively, we believe that the contributions of Li intercalation during overcharge increase with the amount of amorphous or disordered carbon on the surface. These effects can be estimated by investigating the relationship between the overcharge capacity and the amount of deposited Li as measured by ^{7}Li NMR [25].

3.3. Change of graphite surface after grinding

There were many efforts of graphite surface modification by mechanical and chemical treatment for improving electrochemical properties as already mentioned. However, there is little literature about Li deposition morphologies after overcharge, so we focused on the relationship between Li deposition morphologies and the surface condition of graphite. We selected AG1, which is a highly crystalline graphite, and modified its surface using the grinding method. Several samples of AG1 after grinding with different surface conditions were prepared by changing the grinding clearance from 40 to 100 μm, denoted as AG1-40, AG1-60, and AG1-100.

Fig. 4 shows the comparison of Raman spectra of AG1 before and after grinding. The peaks around 1360 cm^{-1}, which are attributed to the disordered carbon, increased due to the decrease in the grinding clearance. As shown in Table 1, the *R*-values of AG1-100, AG1-60, and AG1-40 were 0.24, 0.30, and 0.63, respectively. It was also reported that the peak around 1360 cm^{-1} increased after ballmilling with treating time [14,15].

On the other hand, d_{002} spaces measured with X-ray diffraction showed little change and were about 0.335 nm before and after grinding. It is generally known that graphite has two types of crystal structures, hexagonal (2H, ABAB stacking) and rhombohedral (3R, ABCABC stacking) [26,27]. The hexagonal stacking easily converts to a rhombohedral stacking by a mechanical shock such as during the pulverization process, and the proportion of the rhombohedral crystal increases up to ca. 33 vol% [28,29]. Because of this, we investigated whether the proportion of the rhombohedral crystal in AG1 increased after grinding.

Fig. 5 shows X-ray diffraction patterns of AG1 before and after grinding. Two peaks appeared around 43° and 46°, which were attributed to the rhombohedral crystal structure, hardly changed. This indicated the grinding treatment did not increase the proportion of the rhombohedral crystal structure in the graphite, and

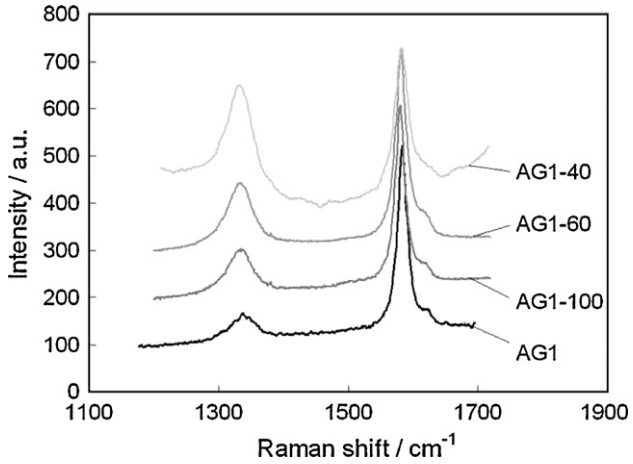

Fig. 4. Raman spectra profiles of AG1 ground with different clearances. AG1; as received, AG1-40, -60, and -100; ground with 40-, 60-, and 100-μm clearance, respectively.

the bulk crystallinity of ground AG1 had not changed. Therefore, we measured the thermogravimetry (TG) of AG1 before and after grinding to investigate the surface condition, based on reports that low crystalline carbon burns out at a lower temperature than high crystalline carbon in air [30,31]. Fig. 6 shows the TG profiles of AG1 before and after grinding. The TG profile of AC was added in Fig. 6 as a reference. As shown in Fig. 6, the starting burnout temperature of AG1-60 was about 660 °C, and it completely disappeared by 840 °C. The TG profile of AG1-60 shifted about 20 °C lower that of AG1 because it had a small amount of disordered carbon created from grinding. Furthermore, we investigated the changes in AG1 and AG1-60 features before and after heating at 700 °C in air. Before and after heat treatment, AG1 showed massive particles of flaky graphite (Fig. 7(a) and (b)), and there was little difference between them. However, the particles of AG1-60 after heat treatment (Fig. 7(d)) were eroded from the edge while the particles of AG1-60 before heat treatment (Fig. 7(c)) were the same as those of AG1. It was assumed that selective burning of disordered carbon from grinding created the above particle features [30].

3.4. Electrochemical properties of graphite after grinding

We measured reversible and irreversible capacities of AG1-100, AG1-60, and AG1–40 to examine the grinding effects on

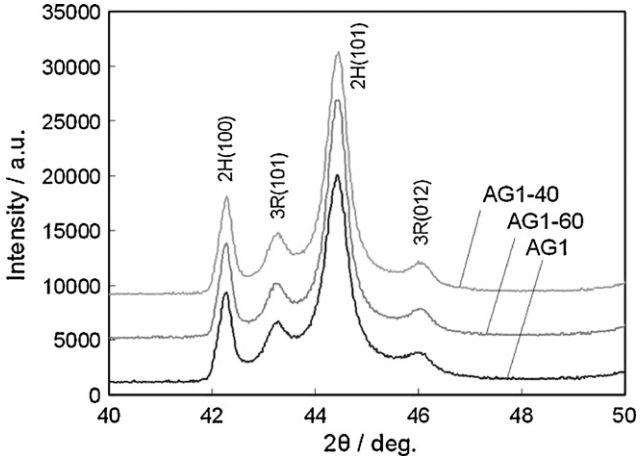

Fig. 5. X-ray diffraction patterns of AG1, AG1-40, and AG1-60, respectively.

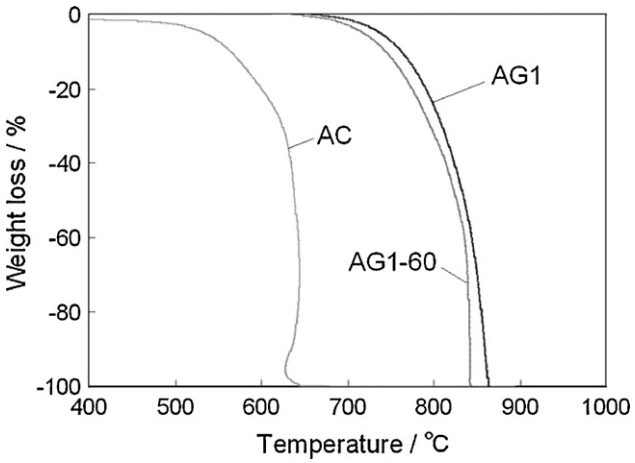

Fig. 6. TG profiles of AG1, AG1-60, and AC at 5 °C min^{-1} from room temperature to 900 °C in air, respectively.

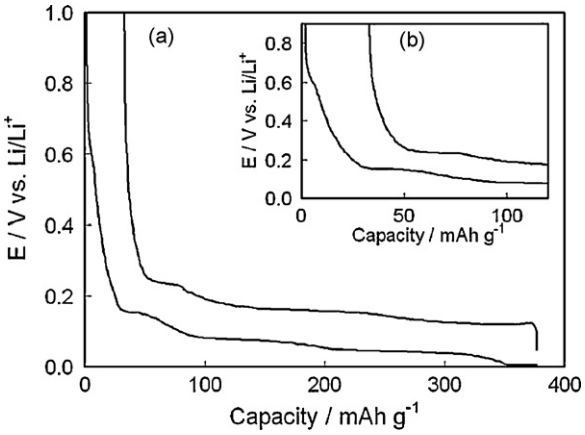

Fig. 8. Intercalation and deintercalation curves of AG1 at first cycle in 1 M $LiPF_6$ EC/DMC (1:2).

electrochemical properties. As shown in Table 1, while their reversible capacities were almost same at about 350 mAh g^{-1}, their irreversible capacities were different depending on the grinding condition. However, there was a decrease of irreversible capacity after grinding, and the irreversible capacity of AG1-60 was at a minimum (28 mAh g^{-1}).

It is generally known that side reactions occur particularly at the first cycle and cause irreversible capacity. Therefore, we investigated the side reactions of AG1 before and after grinding. Fig. 8 shows charge–discharge curves of AG1 at the first cycle. The shoulder between 1.0 to 0.6 V in Fig. 8(b) was caused by the side reactions. To analyze this in more detail, we converted the charge curves of AG1, AG1-60, and AG1-40 into differential forms. Two peaks

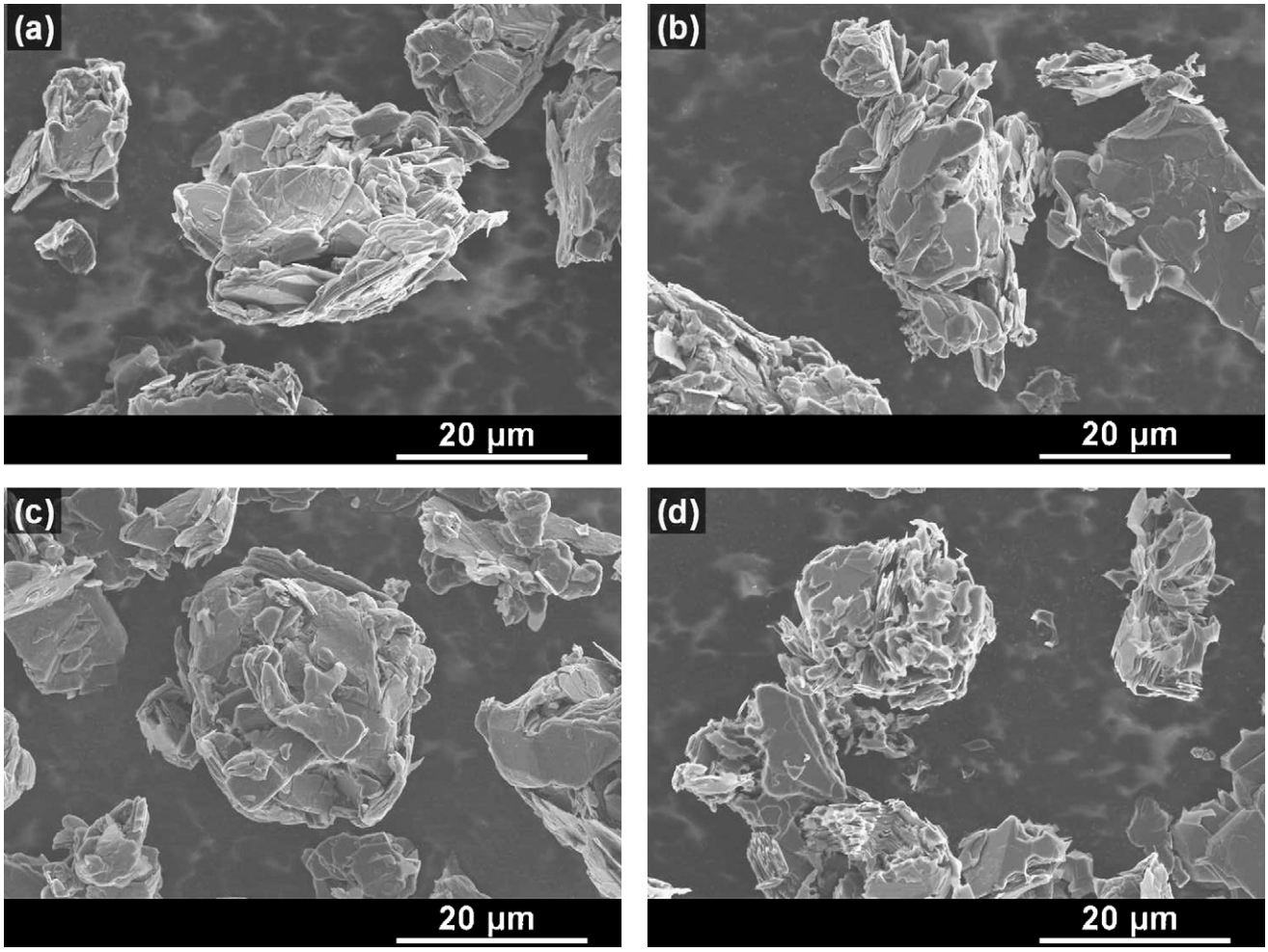

Fig. 7. SEM images of graphite particles before and after heating at 700 °C in air. AG1 particles (a) before and (b) after heating, and AG1-60 particles (c) before and (d) after heating.

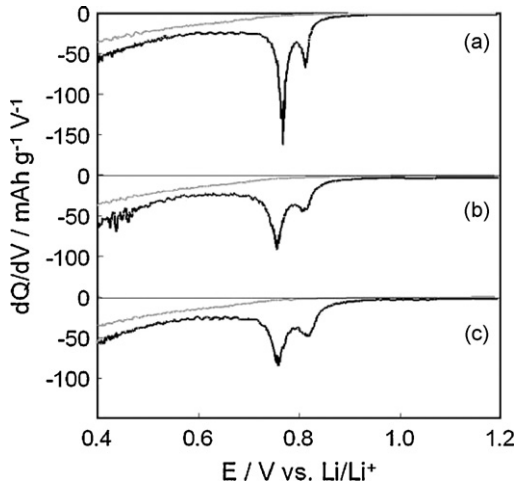

Fig. 9. Differential intercalation curves of (a) AG1, (b) AG1-60, and (c) AG1-40 at in 1 M $LiPF_6$ EC/DMC (1:2). Solid line is first cycle and gray line is second cycle.

appeared between 0.7 and 0.9 V at the first cycle (solid lines in Fig. 9) for all the samples, and these peaks disappeared at the second cycle (gray lines in Fig. 9). We speculate that the first peak at 0.85 V is related to the co-intercalation of solvents with Li ions and their decomposition at the edge plane of graphite. We also speculate that the second peak at 0.75 V is attributed to the decomposition of solvents at the basal plane of graphite from previous literature [3,4]. Moreover, by comparing the differential curves of AG1, AG1-60, and AG1-40 at the first cycle, it was found that the two peaks decreased after grinding.

From these results, we believe that that disordered carbon was created on the graphite surface after grinding without a significant change in bulk crystallinity because the *R*-value increased from 0.10 to 0.63 after grinding to 40 μm, though d_{002} spaces and the proportion of the rhombohedral crystal structure hardly changed. Therefore, the reversible capacities of ground AG1 did not change. On the other hand, the irreversible capacities of ground AG1 would be suppressed by disordered carbon on the surface, which is not more active to electrolyte decomposition than graphite. This is based on previous reports that irreversible capacity of mesocarbon micro beads increases after their turbostratic surface regions are removed by burning out [30]. However, in AG1-40, it was assumed that the decrease of the irreversible capacity was canceled due to

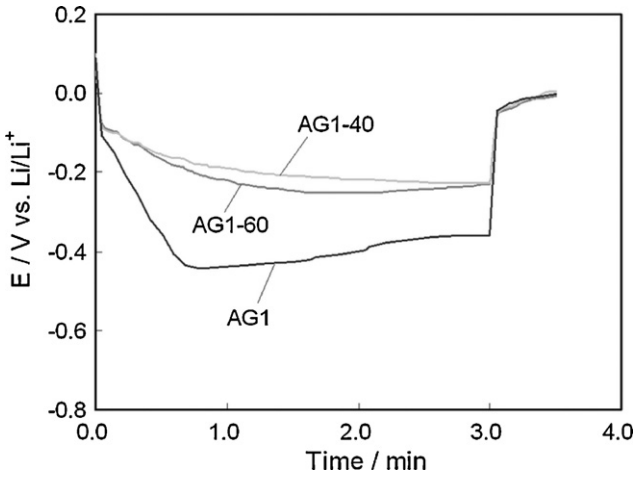

Fig. 10. Potential curves of AG1, AG1-60, and AG1-40 during overcharge at 8.5 mA cm^{-2} for 3 min in 1 M $LiPF_6$ EC/DMC (1:2).

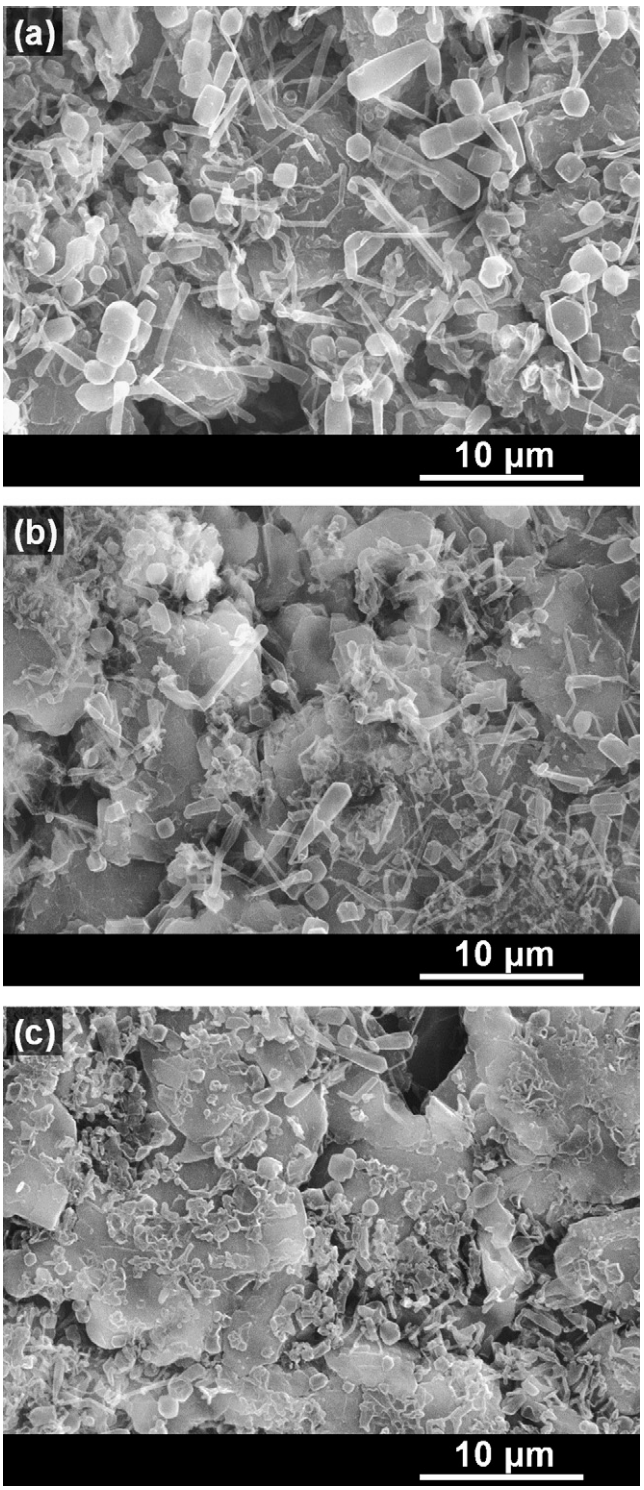

Fig. 11. SEM images of (a) AG1; (b) AG1-60; (c) AG1-40 after Li deposition.

the increase of its surface area from grinding with a narrow clearance.

We investigated the grinding effect on Li deposition morphologies after overcharge. Fig. 10 shows the electrode potentials of AG1-40 and AG1-60 during overcharge. The overcharge voltage of AG1-40 and AG1-60 decreased in comparison with AG1, and the minimum potentials of AG1-40 and AG1-60 were −0.23 and −0.25, respectively. The overshoot in potential curve of AG1 was likely due

to the supersaturation of nucleation for Li deposition. However, it is hard to see the difference of supersaturation between the dendritic and granular cases because the potential curves also involved the Li intercalation reactions, as already mentioned.

Fig. 11 shows SEM images of Li deposition morphologies on these electrodes. The amount of dendritic morphologies of ground AG1 was less than that of AG1, and these dendritic morphologies had gradually changed to granular morphologies due to the increase in the *R*-value. The Li deposition on AG1-40 (Fig. 11(c)), whose *R*-value was over 0.6, had almost all granular morphologies. These results correspond to Fig. 3 and can be explained by a proposed model that numerous defects on the ground graphite surface suppress dendritic Li deposition acting as nuclei, which become starting points of electrodeposition. The nature of the defects on the surface are likely the crevices or the textures consisting of cracked hexagonal-net planes in random order, leading to electrochemical active sites of Li deposition. It is also likely that the more granular Li would deposit on precipitation polycrystalline graphite with smaller crystallite due to increasing number of defects.

4. Conclusion

Li deposition morphologies on graphite are affected by the degree of its surface disorder. The increase of *R*-value, which means the increase of disordered carbon on the surface, causes the morphology of Li deposition to change from dendritic to granular. It is believed that the defects on the disordered carbon act as electrodeposition nuclei and prevent Li dendritic formation. We adopted the grinding method with different clearances to modify graphite surface. The ground graphite, which only creates disordered carbon on its surface without a significant change of bulk crystallinity, has the same reversible capacity as pristine graphite. Furthermore, disordered carbon on ground graphite decreases the irreversible capacity suppressing side reactions and preventing Li dendritic deposition.

References

[1] R. Fong, U.V. Sacken, J.R. Dahn, J. Electrochem. Soc. 137 (1990) 2009.
[2] G.C. Chung, S.H. Jun, K.Y. Lee, M.H. Kim, J. Electrochem. Soc. 146 (1999) 1664.
[3] M. Inaba, Z. Siroma, A. Funabiki, Z. Ogumi, Langmuir 12 (1996) 1535.
[4] S.K. Jeong, M. Inaba, T. Abe, Z. Ogumi, J. Electrochem. Soc. 148 (2001) A989.
[5] E. Peled, C. Menachem, D. Bar-Tow, A. Melman, J. Electrochem. Soc. 143 (1996) L4.
[6] S.K. Jeong, M. Inaba, R. Mogi, Y. Iriyama, T. Abe, Z. Ogumi, Langmuir 17 (2001) 8281.
[7] H. Honbo, Y. Muranaka, F. Kita, Electrochemistry 69 (2001) 686.
[8] A. Du Pasquier, F. Disma, T. Bowmer, A.S. Gozdz, G. Amatucci, J.–M. Tarascon, J. Electrochem. Soc. 145 (1998) 472.
[9] M.N. Richard, J.R. Dahn, J. Electrochem. Soc. 146 (1999) 2068.
[10] D.D. MacNeil, D. Larcher, J.R. Dahn, J. Electrochem. Soc. 146 (1999) 3596.
[11] A.M. Andersson, K. Edstrom, J. Electrochem. Soc. 148 (2001) A1100.
[12] R.A. Leising, M.J. Palazzo, E.S. Takeuchi, K.J. Takeuchi, J. Electrochem. Soc. 148 (2001) A838.
[13] F. Disma, L. Aymard, L. Dupont, J.–M. Tarascon, J. Electrochem. Soc. 143 (1996) 3959.
[14] T.S. Ong, H. Yang, J. Electrochem. Soc. 149 (2002) A1.
[15] C. Natarajan, H. Fujimoto, A. Mabuchi, K. Tokumitsu, T. Kasuh, J. Power Sources 92 (2001) 187.
[16] M. Yoshio, H. Wang, K. Fukuda, Y. Hara, Y. Adachi, J. Electrochem. Soc. 147 (2000) 1245.
[17] T. Doi, K. Takeda, T. Fukutsuka, Y. Iriyama, T. Abe, Z. Ogumi, Carbon 43 (2005) 2352.
[18] I.R.M. Kottegoda, Y. Kadoma, H. Ikuta, Y. Uchimoto, M. Wakihara, Electrochem. Solid-State Lett. 5 (2002) A275.
[19] G. Katagiri, H. Ishida, A. Ishitani, Carbon 26 (1988) 565.
[20] K. Zaghib, G. Nadeau, K. Kinoshita, J. Electrochem. Soc. 147 (2000) 2110.
[21] N. Takami, A. Satoh, T. Ohsaki, M. Kanda, J. Electrochem. Soc. 145 (1998) 478.
[22] K. Kanamura, S. Shiraishi, Z.–I. Takehara, J. Electrochem. Soc. 141 (1994) L108.
[23] S. Shiraishi, K. Kanamura, Z.–I. Takehara, J. Electrochem. Soc. 146 (1999) 1633.
[24] I. Yoshimatsu, T. Hirai, J.–I. Yamaki, J. Electrochem. Soc. 135 (1988) 2422.
[25] M. Letellier, F. Chevallier, F. Beguin, E. Frackowiak, J.-N. Rouzaud, J. Phys. Chem. Solids 65 (2004) 245.
[26] H. Shi, J. Barker, M.Y. Saidi, R. Koksbang, J. Electrochem. Soc. 143 (1996) 3466.
[27] F. Cao, I.V. Barsukov, H.J. Bang, P. Zaleski, J. Prakash, J. Electrochem. Soc. 147 (2000) 3579.
[28] K. Guerin, A. Fevrier-Bouvier, S. Flandrois, M. Couzi, B. Simon, P. Biensan, J. Electrochem. Soc. 146 (1999) 3660.
[29] H.P. Boehm, R.W. Coughlin, Carbon 2 (1964) 1.
[30] K. Suzuki, T. Hamada, T. Sugiura, J. Electrochem. Soc. 146 (1999) 890.
[31] H. Wang, M. Yoshio, T. Abe, Z. Ogumi, J. Electrochem. Soc. 149 (2002) A499.